Available online at www.sciencedirect.com
ScienceDirect
Trans. Nonferrous Met. Soc. China 27(2017) 2587−2597
Transactions of Nonferrous Metals Society of China
www.tnmsc.cn

Effect of thermal-mechanical processing on microstructure and mechanical properties of duplex-phase Mg−8Li−3Al−0.4Y alloy

Hong-bo DING[1], Qiang LIU[1], Hai-tao ZHOU[1], Xiao ZHOU[2], Andrej ATRENS[3]

1. School of Materials Science and Engineering, Central South University, Changsha 410083, China;
2. School of Materials Science and Engineering, McGill University, Montréal, Québec, H3A 0C5, Canada;
3. Division of Materials Engineering, School of Mechanical and Mining Engineering, The University of Queensland, Brisbane, QLD 4072, Australia

Received 15 April 2017; accepted 8 June 2017

Abstract: The effect of thermal-mechanical processing on the microstructure and mechanical properties of the duplex phase Mg−8Li−3Al−0.4Y alloy was investigated. The as-cast alloy was composed of *α*-Mg, *β*-Li, AlLi, Al_2Y and $MgAlLi_2$ phases. Annealing of the cold rolled alloy at 350 °C for 60 min was considered to be optimum. This caused full static recrystallization and spheroidization. A significant *β*-Li loss occurred when the annealing time was increased to 90 min. The optimized annealing treatment produced the following values of the yield strength, ultimate strength and elongation: 148 MPa, 184 MPa and 35%, respectively. The texture evolution of the *α*-phase and the *β*-phase changed remarkably during thermal-mechanical processing.
Key words: Mg−Li alloy; recrystallization; spheroidization; *β*-Li loss; texture

1 Introduction

Magnesium and its alloys, as the lightest structural materials ($\rho\approx1.74$ g/cm^3), are widely of interest for applications in automotive, aerospace, defense and computers [1−4]. However, one problem that inhibits more widespread application of wrought magnesium alloys is the limited ductility and, in particular, poor room temperature formability of current commercial alloys [5,6]. The limited plasticity of traditional Mg alloys is attributed to their hexagonal close-packed (HCP) crystal structure, which has insufficient independent slip systems in the von Mises criteria [5,7]. To overcome this problem, microstructural refinement and the use of alloying elements are possible methods to improve room-temperature formability of Mg alloys [8−13].

Increasing the lithium alloying content changes the crystal structure of Mg alloys: 1) the *c*/*a* ratio is decreased [14] and 2) new phases occur. The Mg−Li equilibrium phase diagram indicates that 1) the Mg-rich *α*-phase (with HCP structure) occurs for Li content less than 5.5% (mass fraction) and 2) the Li-rich *β*-phase (with body-centered cubic (BCC) structure) occurs for Li content greater than 10.3% (mass fraction) [10]. The Li rich *β*-phase is likely to be more ductile. The *c*/*a* ratio decreases from 1.624 for pure Mg to 1.607 for Mg−5.5%Li (mass fraction), which decreases the critical resolved shear stress (CRSS) for slip systems and makes slip systems more easily activated at lower temperatures. So, Mg−5.5%Li (mass fraction) enjoys good formability, which enables the alloy to be easily rolled and annealed. During thermo-mechanical processing, Mg−Li alloys easily undergo recrystallization and recovery, i.e., dynamic recrystallization (DRX), static recrystallization (SRX) and dynamic recovery (DRV), which influences the microstructure, crystallographic texture, anisotropy and mechanical properties [15]. Typically, the texture, i.e. the distribution of crystallographic orientations, is not random, and influences the mechanical properties [16,17]. In recent years, texture evolution of Mg alloys has been extensively investigated, especially for the commercial AZ31 [18−20] and AZ91 [21] alloys. However, the research on Mg−Li alloys has mainly

Foundation item: Project (51461018) supported by the National Natural Science Foundation of China; Projects (20133BAB20008, 20144ACB20013) supported by the Key Program of Natural Science Foundation of Jiangxi Province, China; Project (20151BDH80006) supported by the International Science and Technology Cooperation Program of Jiangxi Province, China
Corresponding author: Hai-tao ZHOU; Tel/Fax: +86-731-88876692; E-mail: htzhou@csu.edu.cn
DOI: 10.1016/S1003-6326(17)60286-3

focused on the smelting process and the mechanical properties [22]. The systematic investigations on texture and texture evolution of Mg−Li alloys are rare, especially for duplex-phase Mg−Li−X alloys.

The present work focuses on the duplex-phase Mg−8Li−3Al−0.4Y alloy, and explores the influence of thermal-mechanical processing on the microstructure and properties. Some conclusions of this work are useful for the development of new Mg−Li−X alloys.

2 Experimental

Commercial pure magnesium (>99.9%), pure lithium (>99.9%), pure aluminum (>99.9%) and Mg−30%Y (mass fraction) master alloy were melted in an electric resistance furnace. Table 1 presents the chemical composition of the as-cast Mg−8Li−3Al−0.4Y alloy as determined by inductively coupled plasma atomic emission spectroscopy (ICPAES).

Table 1 Chemical composition of Mg−8Li−3Al−0.4Y alloy (mass fraction, %)

Li	Al	Y	Mg
7.70	2.93	0.36	Bal.

Experimental specimens, with a size of 100 mm × 180 mm × 10 mm, were taken from the central part of the homogenized ingot, and were wrapped by a 6 μm-thick Al foil to prevent surface oxidation. Hot-rolling was performed at 280 °C to a total cumulative reduction of 80% using a four-pass rolling schedule (20% per pass), all in the same direction, with a heat treatment at 280 °C for 30 min between passes. Cold-rolling was conducted in six successive passes (10% per pass) with a 50% total thickness reduction. Annealing was carried out at 350 °C for 60 min before cold rolling and post-annealing was conducted at temperatures between 250 and 350 °C for 30−90 min.

Specimens for optical microscopy were polished and etched with 3% nital. The grain size was measured by the linear intercept method. The chemical microanalysis of phases was carried out by using energy dispersive spectroscopy (EDS) in the scanning electron microscope (SEM). Phase identification and texture measurement were performed using X-ray diffraction. The tensile tests were conducted along the rolling direction at a speed of 1 mm/min at room temperature.

3 Results and discussion

3.1 Microstructure

Figure 1 shows the XRD pattern of the as-cast Mg−8Li−3Al−0.4Y alloy. Previous work [13] suggested that the Mg−8Li−3Al−0.4Y alloy consisted of the five phases: α-Mg, β-Li, AlLi, Al_2Y and $MgAlLi_2$. In addition, small whitish grains of the Mg-rich α-phase were embedded in the darker Li-rich β phase.

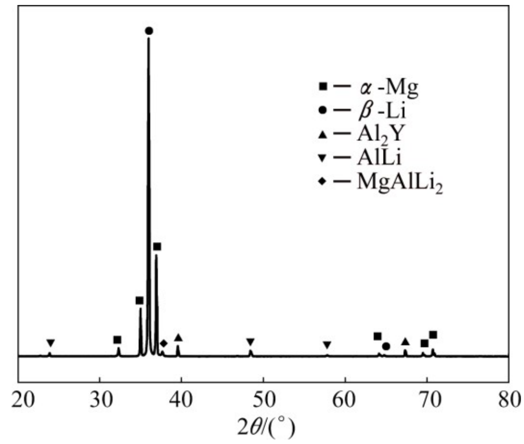

Fig. 1 XRD pattern of as-cast Mg−8Li−3Al−0.4Y alloy

Figure 2 shows optical micrographs of hot-rolled, cold-rolled and annealed Mg−8Li−3Al−0.4Y alloy sheet. Figure 2(a) shows that, after hot rolling, the grains were refined, and the α-phase was elongated in the rolling direction, aligned in the rolling direction, and slightly broken. Figure 2(b) shows that, after hot rolling and annealing, there was some coarsening of the microstructure. In contrast, after cold rolling, the strip and blockily-distributed α-phases were dissociated into a disconnected fragmentized island morphology. Some phase particles were spheroidized with bamboo-like structures after annealing. The cold-rolled specimens contained no visible porosity or open cracks, suggesting good ductility. Figure 2(d) demonstrates that after cold-rolling process, the α phase and β phase were seriously deformed and exhibited a slender micro-structure.

Figure 3 indicates that there was coarsening of the microstructure with increasing temperature and time. At low temperatures with little time shown in Figs. 3(a), (b) and (d), there was no significant difference in the morphology of the α-phase of the cold-rolled specimens. This indicated that no recrystallization had taken place after the low-temperature annealing. After annealing at 250 °C for 90 min and at 300 °C for 60 min, the zigzag structure appeared along the boundaries of the α-phase and several fine fibrous α-phase grains have been fused into spherical particles, as shown in Figs. 3(c) and (e). With increasing the annealing time, the spheroidization of the α-phase increased. Figure 4 also shows the spheroidization and recrystallization of the alloy. For example, at the higher temperature for 60 min (Figs. 3(h) and 4(b)), a majority of fine fibrous α-phases were changed into a spherical structure, while coarse α-phases developed into bamboo-shaped microstructures.

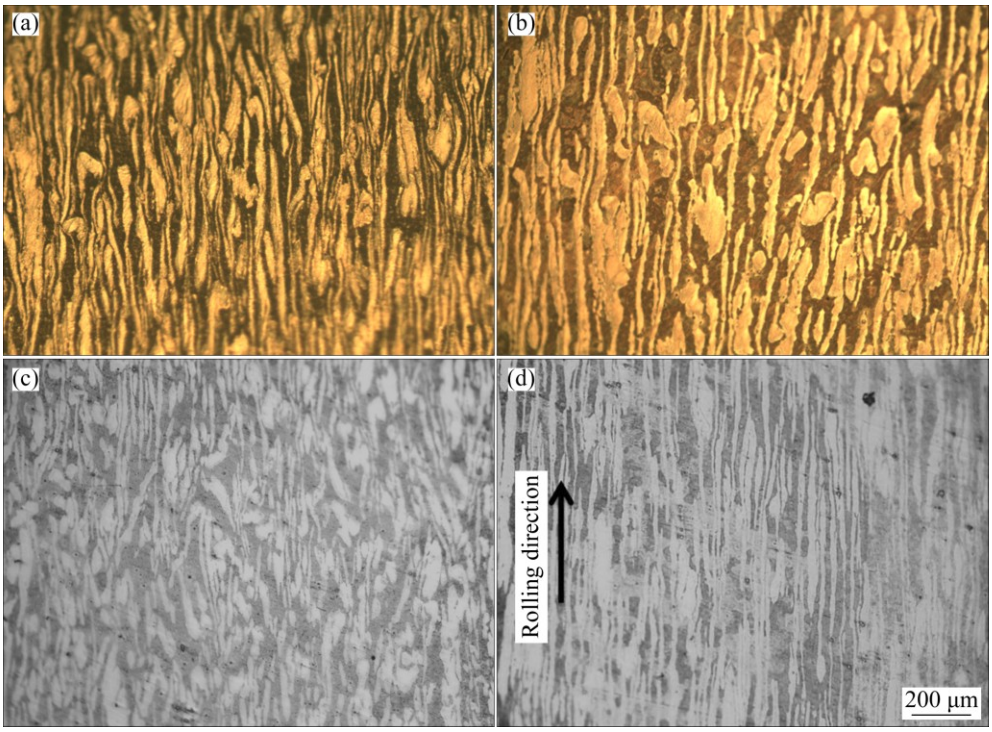

Fig. 2 Optical micrographs of hot-rolled Mg−8Li−3Al−0.4Y alloy sheet with 80% reduction (a), annealed hot-rolled alloy sheet at 350 °C for 1 h (b), and cold-rolled alloy sheet on cross section (c) and longitudinal section (d)

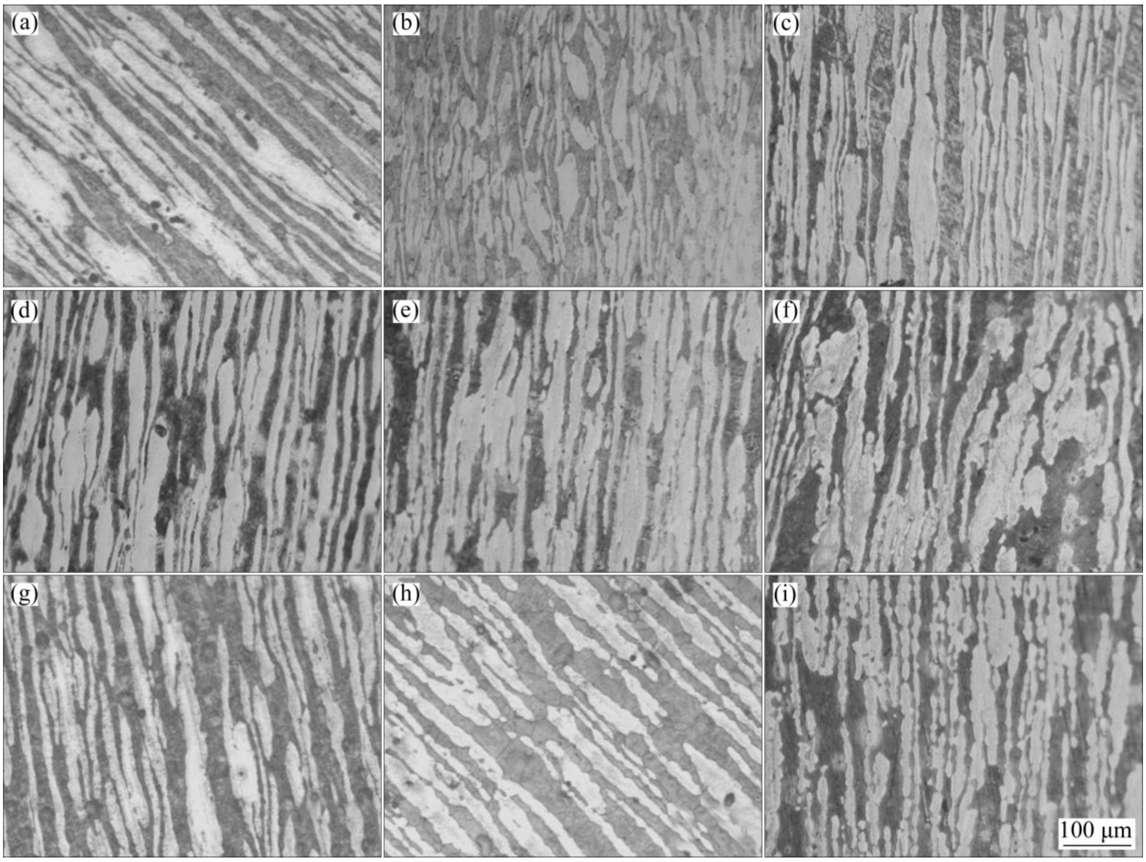

Fig. 3 Optical micrographs of cold-rolled Mg−8Li−3Al−0.4Y alloy sheet annealed under different conditions: (a) 250 °C, 30 min; (b) 250 °C, 60 min; (c) 250 °C, 90 min; (d) 300 °C, 30 min; (e) 300 °C, 60 min; (f) 300 °C, 90 min; (g) 350 °C, 30 min; (h) 350 °C, 60 min; (i) 350 °C, 90 min

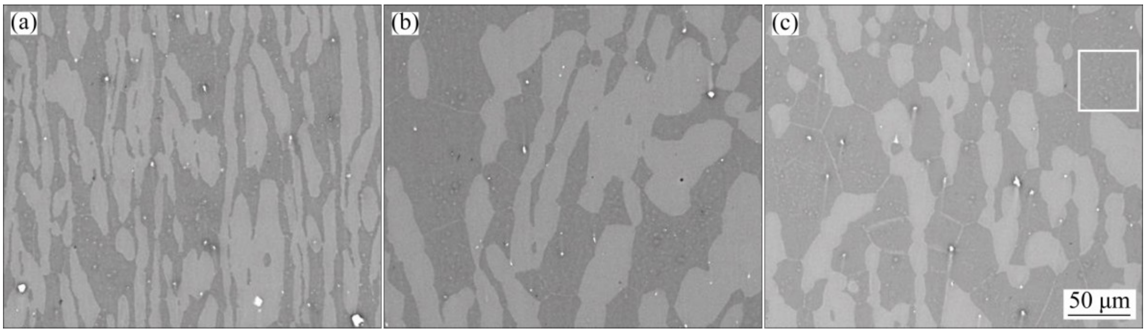

Fig. 4 SEM micrographs of cold-rolled Mg−8Li−3Al−0.4Y alloy sheet (a), and annealed alloy at 350 °C for different time: (b) 60 min; (c) 90 min

Moreover, new equiaxial grains were formed within the β-phase particles at 350 °C, as illustrated in Figs. 4(b) and (c). Spheroidization of all fibrous α-phases occurred after heat treatment for 90 min at 350 °C. In addition, the average size of the spheroidized particles after heat treatment for 90 min at 350 °C was smaller than that of the particles after heat treatment for 60 min. Moreover, a large number of unknown fine acicular phase particles appeared in the β-phase after 90 min at 350 °C, such as those within the white rectangular in Fig. 4(c).

Recrystallization was relatively complete after annealing at 350 °C for 60 min. The microstructure consisted of fully recrystallized β-grains with a mean grain size of 15−30 μm, and the large amount of fine fibrous α-phase particles had become spherical structures, whereas coarse α-phases had become bamboo-shaped microstructures.

Annealing following cold-rolling has been shown by previous work [13] to cause the emergence of acicular α-phase particles inside the β-phase (as marked by the white rectangle in Fig. 4(c)) during heat treatment at the higher temperature (350 °C) or longer time (90 min). Because these particles were precipitated from the β phase, these particles are α phases, and are developed from β phase because of Li loss. Li loss can occur during the heat treatment of Mg−Li alloys [23−26]. The Li can diffuse from inside the specimen to the surface and can be oxidized in air or can sublime in vacuum or in an inert gas environment. CAO et al [24] revealed that Li loss can be attributed to the different atomic mobilities of Mg and Li in the α-phase and β-phase, because the diffusion coefficient of Li in the β-phase is much higher than that of Li in the α-phase and Mg in the β-phase and the α-phase. This phenomenon can also be clearly explained by the following Einstein equation [27] and Arrhenius equation [13] as

$$B=D/(kT) \tag{1}$$

$$D = D_0 \exp\left(-\frac{Q}{RT}\right) \tag{2}$$

where B is the atomic mobility, T is the annealing thermodynamic temperature, k is Boltzmann's constant, D_0 is a constant, Q is the diffusion activation energy, R is the ideal gas constant and D is the diffusion coefficient which depends on the temperature, composition of the alloy and the size of the grains [27]. The ratio of the diffusion coefficient D is equal to the ratio of atomic mobility B when annealing temperature is constant as shown by Eq. (1). Hence, the atomic mobilities of Li and in the β-phase are higher than those of Mg and in the α-phase. Thus, Li loss occurs in the β-phase, resulting in the decrease of the Li content in the β-phase. The application of the "metallographic lever rule" to the binary Mg−Li equilibrium phase diagram can predict the volume fraction of α-phase in the alloy after Li loss. The volume fraction of α-phase increases in the alloy and the volume fraction of β-phase decreases.

Equation (2) indicates that diffusion is accelerated as the temperature rises. Thus, the higher temperature of heat treatment results in more Li loss from the alloy. Such microstructural changes influence both the electrical and mechanical properties of the alloy [24,25], especially for a thin alloy sheet. However, there is no effective method to prevent Li loss. Therefore, it is critical to find the proper annealing temperature as well as time of the rolling process for the Mg−Li alloy.

Partial recrystallization and relatively full recrystallization occurred in the alloy when the alloy was annealed at 300 °C for 60 min and at 350 °C for 60 min, respectively, while the alloy suffered a serious Li loss when the annealing time was increased to 90 min. The spheroidized phases and recrystallized grains were homogeneously distributed when the specimen was annealed at 350 °C for 60 min and this is considered to be the proper annealing treatment after cold-rolling.

3.2 Texture evolution

3.2.1 Rolling and annealing in single α-phase field

Figure 5 shows the textures for the hot-rolled, cold-rolled and annealed cold-rolled conditions by means of the (0002) pole figures of the α-phase. The respective ODFs are displayed in Fig. 6. Figures 5(a) and 6 show a relatively sharp $(0001)\langle 11\bar{2}0\rangle$ basal texture accompanied with a prismatic texture generated by

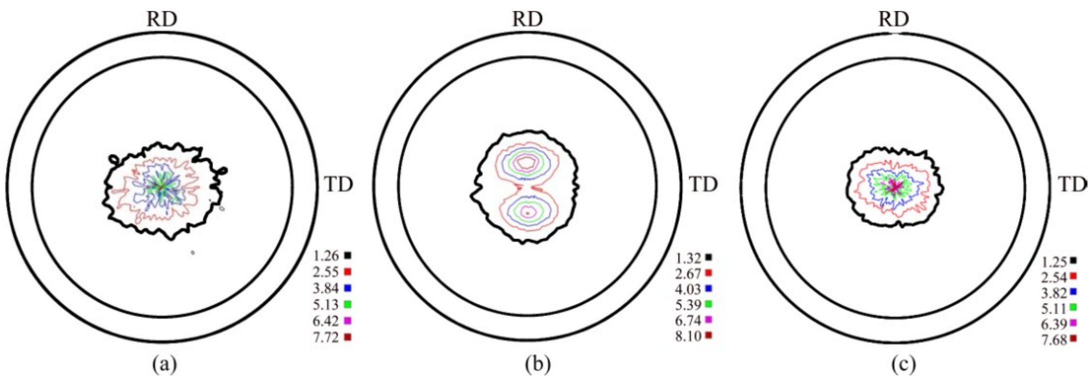

Fig. 5 (0002) pole figures of α phase of hot-rolled (a), cold-rolled (b) and annealed cold-rolled (c) Mg−8Li−3Al−0.4Y alloy

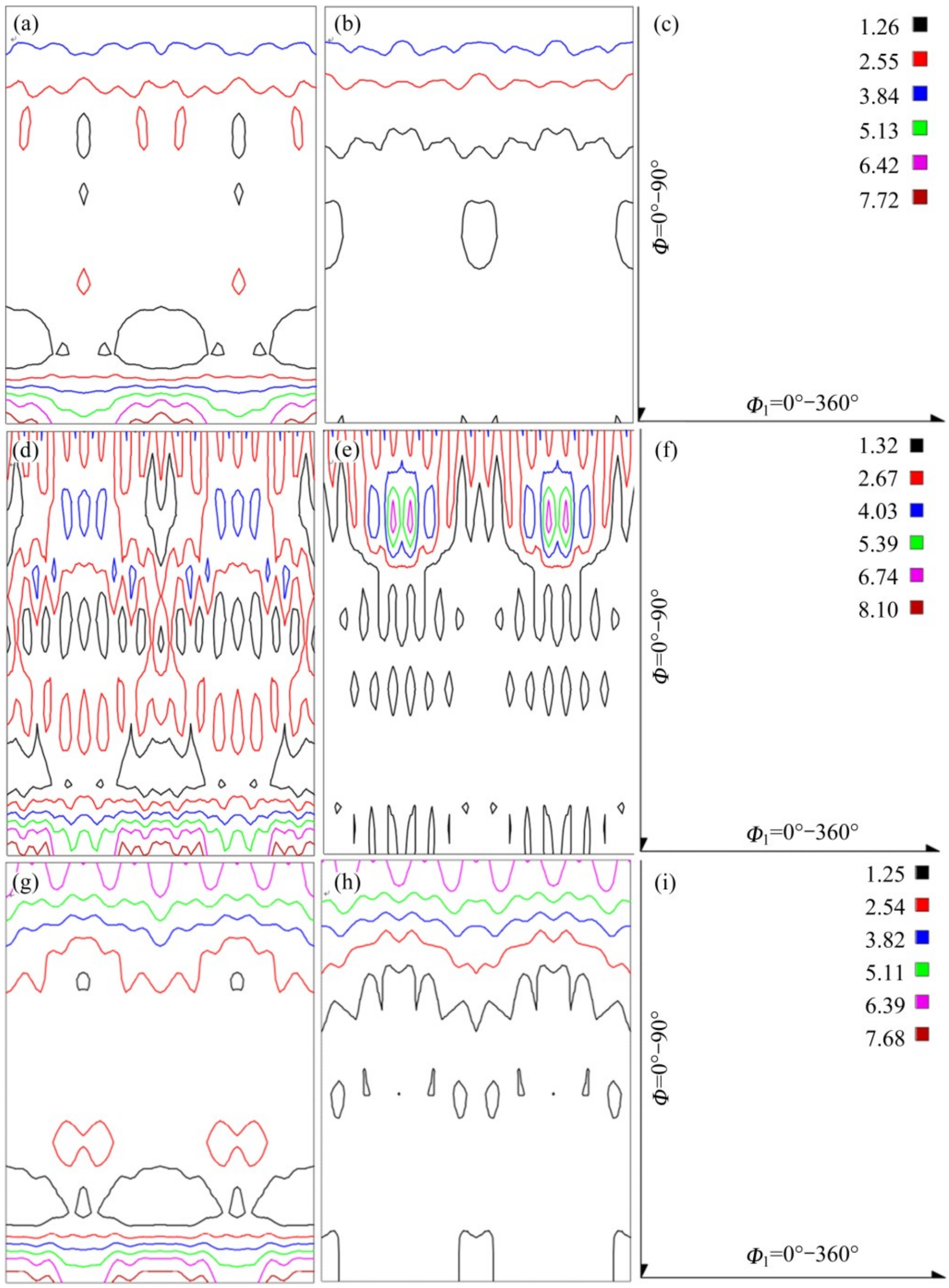

Fig. 6 Constant Φ_2 angle ODF cross-section of α phase of hot-rolled ((a) Φ_2=0°, (b) Φ_2=30° and (c) ruler), cold-rolled ((d) Φ_2=0°, (e) Φ_2=30° and (f) ruler) and subsequent annealed cold-rolled ((g) Φ_2=0°, (h) Φ_2=30° and (i) ruler) Mg−8Li−3Al−0.4Y alloy

hot-rolling. The maximum of the (0002) pole density was 7.72 mrd (multiples of random distribution). The pole density distribution processed by cold-rolling exhibited a double peak, with basal poles rotated away from the normal direction (ND) towards the rolling direction (RD) by ±(15−20)°. WANG and HUANG [16] also suggested that rolling caused the slip plane to gradually rotate toward the rolling plane and the slip direction toward the rolling direction. Figures 6(d)−(f) show the sharper $(0001)\langle 11\bar{2}0\rangle$ basal texture, $\{11\bar{2}0\}\langle 1\bar{1}00\rangle$ prismatic texture, $\{01\bar{1}0\}\langle 10\bar{1}0\rangle$ prismatic texture and high quality $\{11\bar{2}1\}\langle 11\bar{2}2\rangle$ pyramidal texture components generated during cold-rolling. Figure 5(c) demonstrates that the (0002) pole figure of the annealed cold-rolled alloy had a strong (0001) basal texture. In other words, no distinct weakening appeared on $(0001)\langle 11\bar{2}0\rangle$ basal texture after annealing. Furthermore, the peak transferred to the center of pole figure compared with Fig. 5(b), which means that grain-oriented rotation occurred during annealing, making the (0001) crystal plane tend to be parallel to the rolling surface. Figures 6 (g)−(i) indicated that a $\{11\bar{2}1\}\langle 11\bar{2}2\rangle$ pyramidal texture generated during cold-rolling disappeared; however, the intensity of $\{11\bar{2}0\}$ prismatic texture and $\{01\bar{1}0\}$ prismatic texture slightly increased after annealing.

The hot-rolled texture of the Mg−8Li−3Al−0.4Y alloy was formed by several components: both basal and prismatic ($\{01\bar{1}0\}$ and $\{11\bar{2}0\}$) planes were preferentially parallel to the sheet plane, as shown in Figs. 5(a) and 6. This texture was similar to that described previously for hot-rolled Mg−5Li−1Al−RE (Nd or Y) alloys [28]. According to the Schmid's law [29], basal slip is firstly activated due to its lower CRSS when plastic deformation occurs in Mg alloys, in comparison with other non-basal slip systems, and then the $\{0001\}\langle 11\bar{2}0\rangle$ basal slip results in the basal texture for the alloy sheet. AGNEW et al [2] also suggested, by texture modeling, that basal slip and $\{10\bar{1}2\}$ tensile twinning alone would generate a strong basal texture, with a single peak in the basal poles during plane strain compression, while secondary slip or twinning is necessary to rotate the basal poles away from the sheet normal direction. Considering that basal slip can only provide two independent slip systems as discussed above, non-basal slip systems and twins must be activated to harmonize the plastic deformation. Additionally, the deformation temperature as well as *c*/*a* ratios of various HCP materials strongly affect the activation of the different slip systems [30−33]. RAYNOR [30] confirmed that increasing the hot-rolling temperature is expected to affect the rolling texture because the CRSS for glide of dislocations on non-basal planes is temperature dependent and texture reflects the balance of deformation mechanisms. CHEN [31] also suggested that both CRSSs needed to activate basal slip and prismatic slip systems decrease with increasing deformation temperature, and their values are almost equal at 300 °C. So, basal slip system accompanied with prismatic slip systems can be activated in the alloy sheet during deformation at 300 °C. The main characteristic of the HCP deformation texture could be traced on the basis of basal slip and prismatic slip would become the principal slip systems when the *c*/*a* ratio reaches about 1.6. In this work, the value of *c*/*a* ratio of the Mg−8Li−3Al−0.4Y alloy was 1.6077 evaluated from the XRD results, indicating the occurrence of prismatic slip and the generation of a prismatic texture during hot-rolling. However, when the same alloy is cold-rolled after extrusion, the texture is typical of Mg.

Basal slip and prismatic $\langle a\rangle$ slip systems begin to be activated after extensive plastic deformation, making the basal and prismatic planes of grains of the α-phase parallel to the rolling surface. When the plastic deformation reaches a critical amount, both basal and prismatic slip systems approach "hard orientations", thus $(0001)\langle 11\bar{2}0\rangle$ basal texture, $\{11\bar{2}0\}\langle 1\bar{1}00\rangle$ prismatic texture and $\{01\bar{1}0\}\langle 10\bar{1}0\rangle$ prismatic texture components can be generated during cold-rolling, as shown in Figs. 6(d)−(f). The interfacial angle of hexagonal system equation is written as [34]

$$\cos\varphi=\left[h_1h_2+k_1k_2+\frac{1}{2}\left(h_1k_2+h_2k_1\right)+\frac{3a^2}{4c^2}l_1l_2\right]\Big/\sqrt{\left(h_1^2+k_1^2+h_1k_1+\frac{3a^2}{4c^2}l_1^2\right)\left(h_2^2+k_2^2+h_2k_2+\frac{3a^2}{4c^2}l_2^2\right)} \tag{3}$$

where a and c are lattice constants, φ is the interfacial angle and $\{h_1\ k_1\ l_1\}$, $\{h_2\ k_2\ l_2\}$ represent different crystal faces. The angle between the $\{11\bar{2}0\}$ prismatic plane and the $\{10\bar{1}1\}$ pyramidal plane is 40.3° and the angle between the $\{01\bar{1}0\}$ prismatic plane and the $\{10\bar{1}1\}$ pyramidal plane is 63.8°. Therefore, according to the Schmid's law [29], pyramidal $\langle c+a\rangle$ slip systems turn into favorable orientation when the prismatic slip systems are in the "hard orientations" and then pyramidal $\langle c+a\rangle$ slip systems begin to be activated for the plastic deformation. So, it is the combination of prismatic slip systems and pyramidal slip systems that results in the generation of the $\{11\bar{2}1\}\langle 11\bar{2}2\rangle$ texture.

Figure 5(b) also indicates that the rotation and splitting of the basal pole along the RD occur during cold-rolling. In an investigation of Mg−Li alloys, texture modeling indicated that rotation of basal poles in the RD is associated with the glide of $\langle c+a\rangle$ dislocations on the pyramidal planes, and it was concluded that Li can ease the glide of $\langle c+a\rangle$ dislocations [32]. This conclusion is also supported by the evidence generated by a TEM study of dislocations [35].

The double peak in the basal pole following cold-rolling was replaced by a single peak, as shown in Fig. 5(c). This means that there was an evolution in texture associated with SRX and grain growth [32], which was consistent with the microstructure in Figs. 3 and 4. The evolution of texture was therefore associated with the nucleation of new grains in the small regions of unrecrystallized material that remained following rolling in this work. Meanwhile, according to the oriented growth theory [36], the grain growth rate with a certain orientation is considerably higher than that of other orientated grains when recrystallization occurs in alloys. Thus, probably, in this work, with the development of recrystallization, the grain growth rate with prismatic texture is higher than that with $\{11\bar{2}1\}\langle11\bar{2}2\rangle$ pyramidal texture, and the grains with the $\{11\bar{2}1\}\langle11\bar{2}2\rangle$ pyramidal texture are swallowed up gradually by grains with prismatic texture. Consequently, the $\{11\bar{2}1\}\langle11\bar{2}2\rangle$ pyramidal texture generated during cold-rolling disappears, and the intensity of the $\{11\bar{2}0\}\langle1\bar{1}00\rangle$ prismatic texture and the $\{01\bar{1}0\}\langle10\bar{1}0\rangle$ prismatic texture components slightly increases after annealing.

3.2.2 Rolling and annealing in single *β*-phase field

Figure 7 indicates the ODFs of the *β*-phase of hot-rolled, cold-rolled and annealed cold-rolled specimens where the *α* and *γ* fibers are indicated. The primary texture components were {112}⟨110⟩, {112}⟨111⟩ and {001}⟨110⟩ textures; they remained unchanged during rolling and annealing and displayed good texture heredity. The maximum pole densities of the hot-rolled, cold-rolled and annealed cold-rolled specimens were 4.01, 5.25 and 3.84 mrd, respectively. As expected, the well-defined *α* and *γ* fibers formed during rolling were weakened by annealing at 350 °C for 60 min.

The Li-rich *β*-phase has the BCC structure in the duplex-phase Mg−Li alloys [10]. MAO and ZHANG [37] confirmed that the near {111}⟨110⟩ component, an orientation common to both the α and *γ* fibers in BCC metals [38], begins to be activated after rolling, making

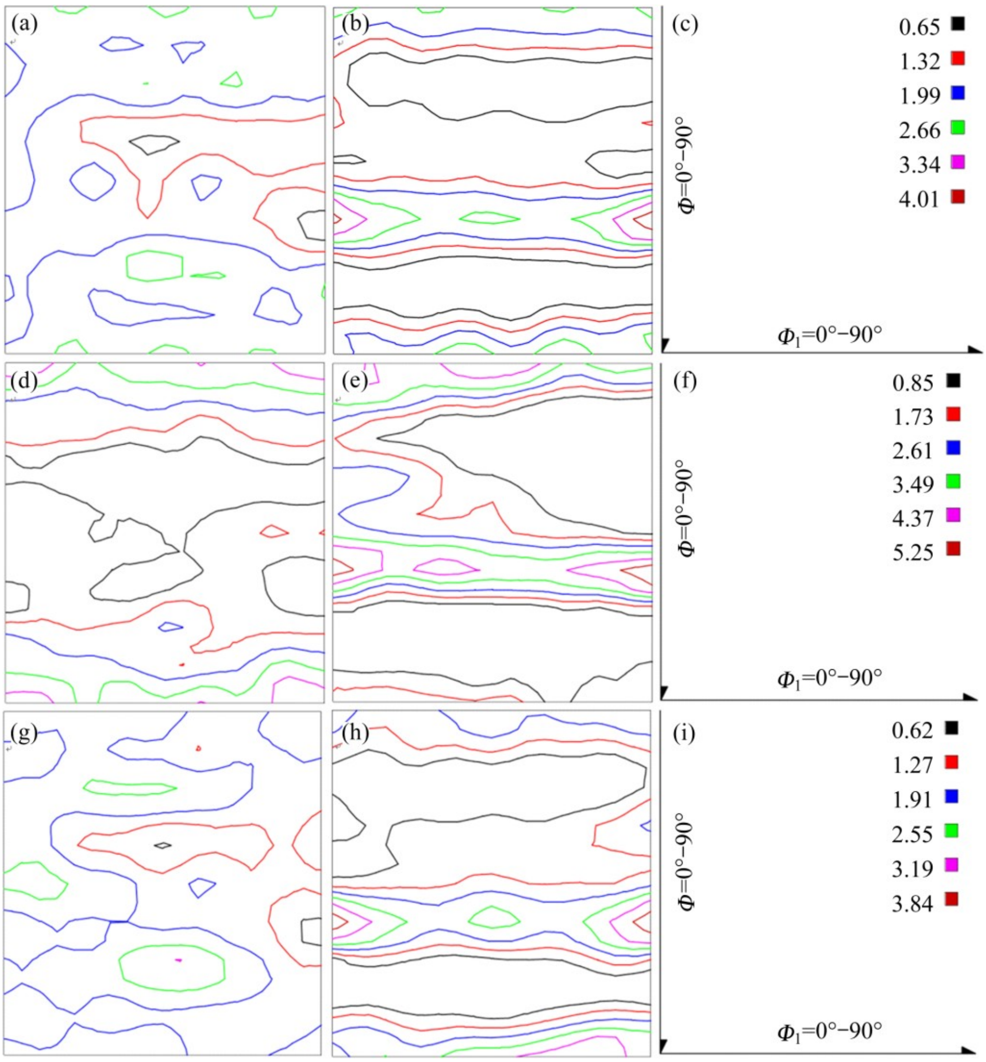

Fig. 7 Constant Φ_2 angle ODF cross-section of *β* phase of hot-rolled ((a) Φ_2=0°, (b) Φ_2=45° and (c) ruler), cold-rolled ((d) Φ_2=0°, (e) Φ_2=45° and (f) ruler) and subsequent annealed cold-rolled ((g) Φ_2=0°, (h) Φ_2=45° and (i) ruler) Mg−8Li−3Al−0.4Y alloy

grain orientations cluster together at the near {001}⟨110⟩ component. Moreover, the grain orientations move along α orientation fiber towards the {112}⟨110⟩ component with increased rolling deformation. The earlier-produced {001}⟨110⟩ cube texture cannot be entirely transformed into the {112}⟨110⟩ texture, and the {001}⟨110⟩ cube texture accompanied with the {112}⟨110⟩ texture was generated during rolling in this alloy, as shown in Fig. 7.

Texture evolution after hot-rolling cannot be eliminated completely during subsequent annealing. During cold-rolling, grain orientations keep flowing to the α and γ fibers on the original basis and make the maximum pole density of cold-rolled alloy higher than that of hot-rolled specimen in {112}⟨110⟩, {112}⟨111⟩, {001}⟨110⟩ texture components. Texture weakening clearly occurred after annealing at 350 °C for 60 min, as shown in Fig. 7. This might be attributed to grain rotation during SRX of the β-phase [39]. The newly-generated grains had no specific orientation relationship with their parent phases, and the parent phases were swallowed up gradually by the newly-generated grains with the progress of recrystallization. Thus, the relatively strong textures in the single β-phase field formed during cold-rolling were weakened by annealing at 350 °C for 60 min, which was similar to the variations in the single α-phase field shown in Fig. 5.

3.3 Mechanical properties

The mechanical properties of Mg−8Li−3Al−0.4Y alloy are presented in Figs. 8 and 9. The tensile yield strength ($\sigma_{0.2}$), ultimate tensile strength (σ_b), Vickers hardness and elongation to failure of different alloys are summarized in Table 2. The work-hardening evolution is evident in Fig. 8 and was consistent with previous literature [14]. The $\sigma_{0.2}$, σ_b, microhardness and elongation of the homogenized alloy were 128 MPa, 142 MPa, HV 62 and 28%, respectively, while those of the hot-rolled alloy with 80% reduction and the cold-rolled alloy with 50% reduction were 170 MPa, 196 MPa, HV 75, 18% and 231 MPa, 266 MPa, HV 86, 11%, respectively. Figure 8 presents representative engineering stress−strain curves of hot-rolled, annealed hot-rolled and cold-rolled Mg−8Li−3Al−0.4Y alloys. All exhibit rapid hardening up to a rather high stress followed by a single transition to slightly lower hardening and flow softening. Figure 9

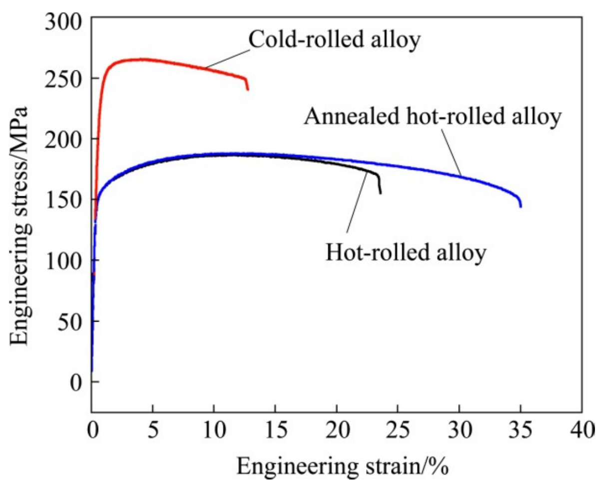

Fig. 8 Tensile curves of hot-rolled, annealed hot-rolled and cold-rolled Mg−8Li−3Al−0.4Y alloy

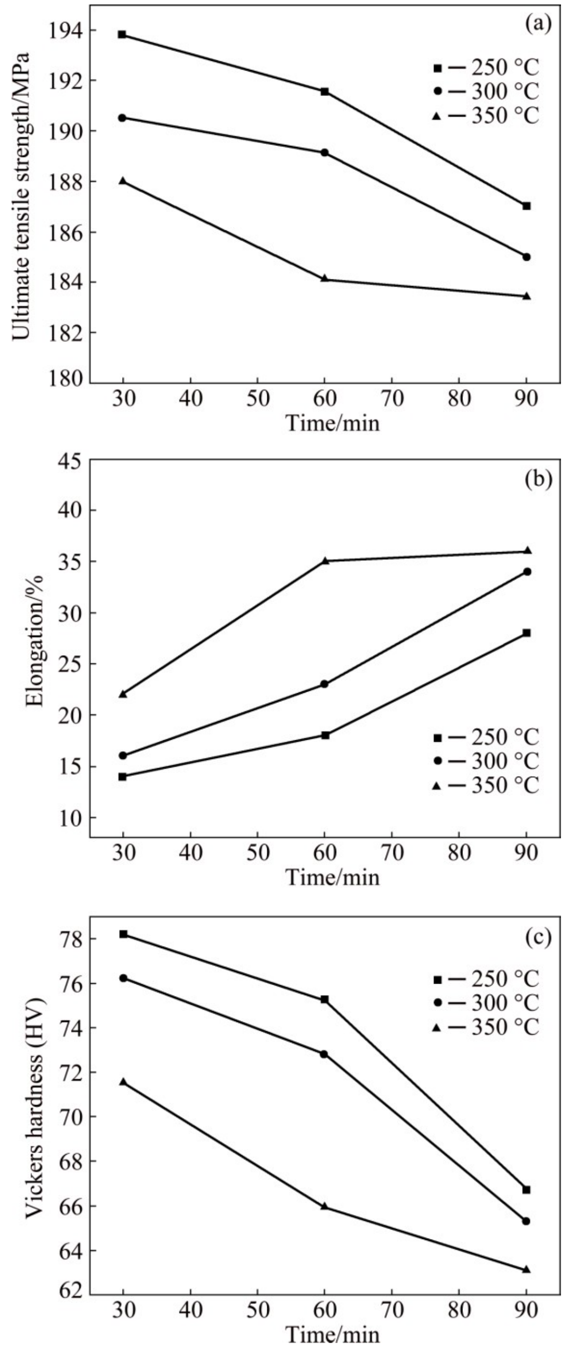

Fig. 9 Influence of annealing temperature and time on mechanical properties of cold-rolled Mg−8Li−3Al−0.4Y alloy sheet: (a) Ultimate tensile strength; (b) Elongation; (c) Vickers hardness

shows that, with increasing annealing time and temperature, the strength and microhardness slightly decreased while the ductility increased. The tensile strength and hardness of the alloy investigated in this work showed comparative values with experimental and commercial Mg−Li alloys [22] and had good elongation as shown in Fig. 9 and Table 2, which reach 34% after annealing.

Table 2 Mechanical properties of homogenized, rolled and annealed Mg−8Li−3Al−0.4Y alloy

State	$\sigma_{0.2}$/ MPa	σ_b/ MPa	Elongation/ %	Microhardness (HV)
Homogenized (300 °C, 12 h)	128	142	28	62
Hot-rolled (80% reduction)	170	196	18	75
Annealed hot-rolled (350 °C, 1 h)	151	188.	34	66
Cold-rolled (50% reduction)	231	266	11	86
Annealed cold-rolled (350 °C, 1 h)	148	184	35	66

For a high annealing temperature and long time, SRX occurs. Defects generated during rolling are eliminated, and softening occurs, as shown in Fig. 9(b). Generally, the α-phase in Mg−Li alloys exhibits a relatively high strength and these bamboo-like α phases refine the grains to a certain extent, while the β-phase shows a better ductility. Considering previous metallographic observation as presented in Figs. 2(b) and 3, many α-phase particles with long strip shape in the rolled alloy were transformed to spherical α-phase particles by annealing. This change of the shape of the α-phase could improve the strength and plasticity of the alloy [13]. Whilst, the grains become coarser and the content of α-phase increases due to Li loss from the β-phase, as shown in Fig. 4(c). Consequently, it is the microstructure of the spherical α-phase particles, coarse grains, grain refinement and the increasing content of α-phase that lead to the values of σ_b, microhardness and elongation.

The σ_b decreased from 266 to 194 MPa, while the elongation increased from 11% to 14%, when the cold-rolled alloy was annealed at 250 °C for 30 min, as shown in Fig. 9 and Table 2. The optical micrographs showed that there was no significant difference in the morphology of the α-phase between cold-rolled specimen and annealed specimen at 250 °C for 30 min, so that recovery occurred first during annealing and decreased strength and microhardness and slightly increased elongation. The σ_b values of the annealed cold-rolled alloys treated at 300 °C for 60 min and at 350 °C for 60 min were almost the same, while the elongation of the latter alloy (annealed at 350 °C for 60 min) was higher than that of the former with a value of 35%. The spherized α-phase and SRX of elongated β-phase played important parts in this increased plasticity. As the annealing time was extended to 90 min, a relatively higher strength distinctly appeared at 350 °C, which principally may be due to Li loss from the alloy so that it affects the mechanical properties of alloy sheet. Therefore, the alloy annealed at 350 °C for 60 min can be considered as the optimal annealing process after cold rolling.

4 Conclusions

1) After thermo-mechanical processing, the Mg−8Li−3Al−0.4Y alloy contained the following five phases: α-Mg, β-Li, AlLi, Al_2Y and $MgAlLi_2$.

2) Annealing at 350 °C for 60 min was considered optimal. This caused spheroidization and complete static recrystallization in the Mg−8Li−3Al−0.4Y alloy. The tensile yield strength, ultimate tensile strength and elongation were 148 MPa, 184 MPa and 35%, respectively. Li loss occurred during annealing at 350 °C for 90 min.

3) The hot-rolled texture of the α-phase of the Mg−8Li−3Al−0.4Y alloy was a combination of $\{0001\}\langle 11\bar{2}0\rangle$ basal texture, $\{11\bar{2}0\}\langle 1\bar{1}00\rangle$ prismatic texture and $\{01\bar{1}0\}\langle 10\bar{1}0\rangle$ prismatic texture. A $\{11\bar{2}1\}\langle 11\bar{2}2\rangle$ pyramidal texture component was generated by cold-rolling with 50% reduction and disappeared during subsequent annealing. The maximum pole densities of the hot-rolled, cold-rolled and annealed cold-rolled specimens were 7.7, 8.1 and 7.7 mrd, respectively.

4) The primary textures of the β-phase of hot-rolled Mg−8Li−3Al−0.4Y alloy were $\{112\}\langle 110\rangle$, $\{112\}\langle 111\rangle$ and $\{001\}\langle 110\rangle$ textures. They remained unchanged during cold-rolling and subsequent annealing. The maximum pole densities of the hot-rolled, cold-rolled and annealed cold-rolled specimens were 4.0, 5.3 and 3.8 mrd, respectively.

References

[1] SUBRAVEL V, PADMANABAN G, BALASUBRAMANIAN V. Effect of welding speed on microstructural characteristics and tensile properties of GTA welded AZ31B magnesium alloy [J]. Transactions of Nonferrous Metals Society of China, 2014, 24: 2776−2784.

[2] AGNEW S R, YOO M H, TOMÉ C N. Application of texture simulation to understanding mechanical behavior of Mg and solid solution alloys containing Li or Y [J]. Acta Materialia, 2001, 49: 4277−4289.

[3] LI M, LOU X Y, KIM J H, WAGONER R H. An efficient constitutive model for room-temperature, low-rate plasticity of annealed Mg AZ31B sheet [J]. International Journal of Plasticity, 2010, 26: 820−858.

[4] LIU Zhi-yi, HUANG Tian-tian, LIU Wen-juan, KANG Sukbong. Dislocation mechanism for dynamic recrystallization in twin-roll casting Mg−5.51Zn−0.49Zr magnesium alloy during hot compression at different strain rates [J]. Transactions of Nonferrous Metals Society of China, 2016, 26: 378−389.

[5] LOU X Y, LI M, BOGER R K, AGNEW S R, WAGONER R H. Hardening evolution of AZ31B Mg sheet [J]. International Journal of Plasticity, 2007, 23: 44−86.

[6] FERDOWSI M R G, MAZINANI M, EBRAHIMI G R. Effects of hot rolling and inter-stage annealing on the microstructure and texture evolution in a partially homogenized AZ91 magnesium alloy [J]. Materials Science and Engineering A, 2014, 606: 214−227.

[7] TAYLOR G I. The mechanism of plastic deformation of crystals. Part I. Theoretical [J]. Proceedings of the Royal Society of London, 1934, 145: 362−387.

[8] KARAMI M, MAHMUDI R. The microstructural, textural, and mechanical properties of extruded and equal channel angularly pressed Mg−Li−Zn alloys [J]. Metallurgical and Materials Transactions A, 2013, 44: 3934−3946.

[9] KOIKE J. Enhanced deformation mechanisms by anisotropic plasticity in polycrystalline Mg alloys at room temperature [J]. Metallurgical and Materials Transactions A, 2005, 36: 1689−1696.

[10] AL-SAMMAN T. Comparative study of the deformation behavior of hexagonal magnesium-lithium alloys and a conventional magnesium AZ31 alloy [J]. Acta Materialia, 2009, 57: 2229−2242.

[11] SON H T, KIM T H, KIM D W, KIM J H, YU H S. Effects of Li addition on the microstructure and mechanical properties of Mg−3Zn−1Sn−0.4Mn based alloys [J]. Journal of Alloys and Compounds, 2013, 564: 130−137.

[12] WANG Bo, CHEN Xian-hua, PAN Fu-sheng, MAO Jian-jun, FANG Yong. Effects of cold rolling and heat treatment on microstructure and mechanical properties of AA 5052 aluminum alloy [J]. Transactions of Nonferrous Metals Society of China, 2015, 25: 2481−2489.

[13] PENG Q Z, ZHOU H T, ZHONG F H, DING H B, ZHOU X, LIU R R, XIE T, PENG Y. Effects of homogenization treatment on the microstructure and mechanical properties of Mg−8Li−3Al−Y alloy [J]. Materials & Design, 2015, 66: 566−574.

[14] DONG Han-wu, PAN Fu-sheng, JIANG Bin, ZENG Ying. Evolution of microstructure and mechanical properties of a duplex Mg-Li alloy under extrusion with an increasing ratio [J]. Materials & Design, 2014, 57: 121−127.

[15] WEI Guo-bing, PENG Xiao-dong, HU Fa-ping, HADADZADEH A, YANG Yan, XIE Wei-dong, WELLS M A. Deformation behavior and constitutive model for dual-phase Mg−Li alloy at elevated temperatures [J]. Transactions of Nonferrous Metals Society of China, 2016, 26: 508−518.

[16] WANG Y N, HUANG J C. Texture analysis in hexagonal materials [J]. Materials Chemistry and Physics, 2003, 81: 11−26.

[17] PROUST G, TOMÉ C N, KASCHNER G C. Modeling texture, twinning and hardening evolution during deformation of hexagonal materials [J]. Acta Materialia, 2007, 55: 2137−2148.

[18] BARNETT. Twinning and the ductility of magnesium alloys: Part I: “Tension” twins [J]. Materials Science and Engineering A, 2007, 464: 1−7.

[19] STANFORD N, SOTOUDEH K, BATE P S. Deformation mechanisms and plastic anisotropy in magnesium alloy AZ31 [J]. Acta Materialia, 2011, 59: 4866−4874.

[20] ANDO D, KOIKE J, SUTOU Y. Relationship between deformation twinning and surface step formation in AZ31 magnesium alloys [J]. Acta Materialia, 2010, 58: 4316−4324.

[21] ROBSON J D, STANFORD N, BARNETT M R. Effect of precipitate shape on slip and twinning in magnesium alloys [J]. Acta Materialia, 2011, 59: 1945−1956.

[22] CHEN Zhao-yun, DONG Zi-chao, YU Chun, TONG Rui. Microstructure and properties of Mg−5.21Li−3.44Zn−0.32Y−0.01Zr alloy [J]. Materials Science and Engineering A, 2013, 559: 651−654.

[23] UEDA H, MATSUI A, FURUKAWA M, MIURA Y, NEMOTO M. Lithium loss during heat treatment of an Al−Li alloy [J]. Journal of Japan Institute of Metals,1985, 49: 562−568.

[24] CAO F R, DING H, LI Y L, ZHOU G, CUI J Z. Superplasticity, dynamic grain growth and deformation mechanism in ultra-light two-phase magnesium−lithium alloys [J]. Materials Science and Engineering A, 2010, 527: 2335−2341.

[25] EL-SALAM F A, EATAH A I, TAWFIK A. Effect of Li loss on some physical properties of Al−Li alloy [J]. Physica Status Solidi A, 1983, 75: 379−384.

[26] RAMAMURTY U, BANDYOPADHYAY A, DWARAKADASA E S. Effect of heat treatment environment on Li depletion and on mechanical properties in Al−Li alloy sheets [J]. Journal of Materials Science, 1993, 28: 6340−6346.

[27] MARCONI U M B, PUGLISI A, RONDONI L, VULPIANI A. Fluctuation-dissipation: Response theory in statistical physics [J]. Physics Reports, 2008, 461:111−195.

[28] ZHU Tian-long, SUN Jian-feng, CUI Chong-liang, WU Rui-zhi, BETSOFEN S, LENG Zhe, ZHANG Jing-huai, ZHANG Mi-lin. Influence of Y and Nd on microstructure, texture and anisotropy of Mg−5Li−1Al alloy [J]. Materials Science and Engineering A, 2014, 600: 1−7.

[29] SCHMID E. Yield point of crystals: Critical shear stress law [M]. Neetherland: Delft, 1924.

[30] RAYNOR G V. The physical metallurgy of magnesium and its alloys [M]. New York: Pergamon, 1959.

[31] CHEN Zhen-hua. Wrought magnesium alloy [M]. Beijing: Chemical Industry Press, 2005 (in Chinese).

[32] MACKENZIE L W F, PEKGULERYUZ M. The influences of alloying additions and processing parameters on the rolling microstructures and textures of magnesium alloys [J]. Materials Science and Engineering A, 2008, 480: 189−197.

[33] XU Tian-cai, PENG Xiao-dong, JIANG Jun-wei, XIE Wei-dong, CHEN Yuan-fang, WEI Guo-bing. Effect of Sr content on microstructure and mechanical properties of Mg−Li−Al−Mn alloy [J]. Transactions of Nonferrous Metals Society of China, 2014, 24: 2752−2760.

[34] PAN Jin-sheng, TIAN Min-bo, TONG Jian-min. Foundation of material science [M]. Beijing: Tsinghua University Press, 2011. (in Chinese)

[35] AGNEW S R, HORTON J A, YOO M H. Transmission electron microscopy investigation of ⟨c+a⟩ dislocations in Mg and α-solid solution Mg−Li alloys [J]. Metallurgical and Materials Transactions A, 2002, 33: 851−858.

[36] KASHYAP K T. On the origin of recrystallization textures [J]. Bulletin of Materials Science, 2001, 24: 23−26.

[37] MAO Wei-min, ZHANG Xin-ming. Quantitative analysis of texture in crystal materials [M]. Beijing: Metallurgical Industry Press, 1993.

[38] SHEN G J, DUGGAN B J. Texture development in a cold-rolled and annealed body-centered-cubic Mg−Li alloy [J]. Metallurgical and Materials Transactions A, 2007, 38: 2593−2601.

[39] ZHANG Ya-ping, JIN Li, DONG Jie, ZHANG Zhen-yan, WANG Yao. Effects of per-pass reduction and annealing treatment on microstructures and mechanical properties of Mg−Zn−Ce−Zr alloy [J]. The Chinese Journal of Nonferrous Metals, 2012, 22: 2985−2991. (in Chinese)

热力过程对双相 Mg−8Li−3Al−0.4Y 合金组织和力学性能的影响

丁洪波[1]，刘 强[1]，周海涛[1]，周 啸[2]，Andrej ATRENS[3]

1. 中南大学 材料科学与工程学院，长沙 410083；
2. School of Materials Science and Engineering, McGill University, Montréal, Québec, H3A 0C5, Canada;
3. Division of Materials Engineering, School of Mechanical and Mining Engineering, The University of Queensland, Brisbane, QLD 4072, Australia

摘　要：研究热力过程对双相 Mg−8Li−3Al−0.4Y 合金组织和力学性能的影响。结果表明，铸态合金含有 α-Mg、β-Li、AlLi、Al_2Y 和 $MgAlLi_2$ 相，经过 350 °C 退火 60 min 处理后，冷轧态合金发生了静态再结晶和球化，当退火时间达到 90 min 时，发生了严重的脱锂。通过优化退火温度和退火时间，得到最佳的退火参数：350 °C 和 60 min，此时合金具有较高的屈服强度(148 MPa)、抗拉强度(184 MPa)和伸长率(35%)。此外，热力过程对 α 相和 β 相的织构演变也具有显著的影响。

关键词：Mg−Li 合金；再结晶；球化；脱锂；织构

(Edited by Bing YANG)